Front. Earth Sci. China 2010, 4(2): 152–159
DOI 10.1007/s11707-010-0018-4

RESEARCH ARTICLE

Features of ferric sulfate precipitates formed by different cultivations of *Acidithiobacillus ferrooxidans*

Xin WANG, Yan LI, Anhuai LU (✉), Changqiu WANG

The Key Laboratory of Orogenic Belts and Crustal Evolution, School of Earth and Space Sciences, Peking University, Beijing 100871, China

Abstract This study focused on the ferric sulfate precipitates formed during the culture of *Acidithiobacillus ferrooxidans* (*A. ferrooxidans*) in a modified 9K medium by applying a potential control on the electrode. X-ray diffraction (XRD), environmental scanning electron microscope (ESEM), Raman spectroscopy (Raman) and Fourier Transform Infrared spectroscopy (FTIR) were carried out to characterize and identify the precipitates which were formed, respectively, in the electrochemical cultivation with a fixed cathode potential (bias-experiment) and in the conventional batch cultivation without cathode potential control (no-bias-experiment). The results indicated that K-jarosite presented in both experiments while NH_4-jarosite and schwertmannite were only found in the no-bias-experiment. The formation of different precipitates could be attributed to the different growth statuses and rates of *A. ferrooxidans* and the different concentrations of Fe^{3+}. In the bias-experiment, external electrons reproduced Fe^{2+} and promoted the growth of *A. ferrooxidans*, thus resulting in the low Fe^{3+} concentration and the rapid depletion of NH_4^+ as the nitrogen source, in which K-jarosite was preferentially formed. In the no-bias-experiment, the lower concentration of *A. ferrooxidans* was observed, which was due to the continuous consumption of Fe^{2+} by bacteria, thus resulting in the relatively higher Fe^{3+} and the NH_4^+ concentration in culture. The high concentration of Fe^{3+} favored the precipitation of the solid solution of K-NH_4-H_3O jarosite, and led to the formation of schwertmannite after K^+ and NH_4^+ were depleted.

Keywords *Acidithiobacillus ferrooxidans*, electrochemical cultivation, schwertmannite, jarosite

Received December 7, 2009; accepted January 18, 2010

E-mail: ahlu@pku.edu.cn

1 Introduction

Acidithiobacillus ferrooxidans (*A. ferrooxidans* or *A. f.*) is a rod-like, chemoautotroph and gram-negative bacterium which was first reported by Colmer et al. (1949). *A. ferrooxidans* usually utilizes ferrous ion and reductive sulfur (Colmer and Hinkle, 1947; Colmer et al., 1949) as its energy resources, in which the pH value can be as low as 2. The oxidation of ferrous ion by *A. ferrooxidans* can be depicted as follows:

$$4Fe^{2+} + O_2 + 4H^+ \xrightarrow{A.f.} 4Fe^{3+} + 2H_2O \qquad (1)$$

The growth of *A. ferrooxidans* can be stimulated by electrochemical cultivation as compared to the conventional batch cultivation. The electrochemical cultivation of *A. ferrooxidans* was operated by using a three-electrode electrochemical system, in which the cathode potential was controlled at a fixed value (Nakasono et al., 1997). The cell concentration in electrochemical cultivation has been reported to be 50–100 folds higher than that in conventional batch cultivation (Blake et al., 1994; Matsumoto et al., 1999). In natural acid environments like acid mineral drainage (AMD), ferric ion, which is the oxidizing product by *A. ferrooxidans*, usually precipitates with sulfate and alkali metal or alkali metal-like ions at extremely low pH value from 1.7 to 4.5 (Bigham et al., 1996; Wang et al., 2007; Dutrizac and Kaiman, 1976). The precipitates are usually some ferric iron oxyhydrosulfate compounds such as schwertmannite [$Fe_8O_8(OH)_6SO_4$] and jarosite [$MFe_3(OH)_6(SO_4)_2$], in which M represents Na^+, K^+, NH_4^+ or H_3O^+ (Drouet and Navrotsky, 2003). Schwertmannite is always poorly crystallized, and often co-exists with the well-crystallized jarosite (Bigham et al., 1996). The following two equations represent their formation processes.

$$8Fe^{3+} + SO_4^{2-} + 14H_2O \rightarrow Fe_8O_8(OH)_6SO_4 + 22H^+ \quad (2)$$

$$M^+ + 3Fe^{3+} + 2SO_4^{2-} + 6H_2O \rightarrow MFe_3(OH)_6(SO_4)_2 + 6H^+ \quad (3)$$

Generally, the pH value ranging from 2.8 to 4.5 (Bigham et al., 1996) favors schwertmannite formation but in some conditions the pH value for schwertmannite formation can also be as low as 2.0 (Wang et al., 2006), while that for jarosite formation can be as low as 1.7 (Dutrizac and Kaiman, 1976).

In terms of the electrochemical cultivation of *A. ferrooxidans*, the growth kinetics of bacteria and the effects of the pH value and the Fe^{2+} concentration on bacterial growth have been previously investigated (Nakasono et al., 1997; Matsumoso et al., 1999). However, less work has been conducted on the precipitates formed in the culture medium. In this study, the features of the precipitates produced in both the electrochemical and the conventional cultivations of *A. ferrooxidans* are characterized by X-ray diffraction (XRD), environmental scanning electron microscope (ESEM), Raman spectroscopy (Raman) and Fourier Transform Infrared spectroscopy (FTIR), and then the mechanisms of the mineral formation are discussed.

2 Materials and methods

2.1 Bacterial preparation

The pure strain of *A. ferrooxidans* applied in this study was offered by the State Key Laboratory for Mineral Deposits Research in Nanjing University. The bacteria were activated and cultured in two 500 mL Erlenmeyer flasks containing 500 mL of modified 9K medium (m9K) with the composition as follows: i.e., 0.15 g/L $(NH_4)_2SO_4$, 0.05 g/L KH_2PO_4, 0.05 g/L KCl, 0.5 g/L $MgSO_4 \cdot 7H_2O$, 0.01 g/L $Ca(NO_3)_2 \cdot 4H_2O$, 41.7 g/L $FeSO_4 \cdot 7H_2O$ (Touvinen and Kelly, 1973). The pH value of the medium was adjusted to 2.0 using 1 M sulfuric acid. The inoculation ratio was 10% (V/V). The flasks were shaken with a rotation speed of 150 rpm at 30°C. The culture was harvested when Fe^{2+} was completely oxidized to Fe^{3+}.

2.2 Electrochemical equipment setup

The electrochemical cultivation of *A. ferrooxidans* was performed by controlling the cathode potential at a fixed value in a three-electrode electrochemical equipment, and presented as bias-experiment. For comparison, the conventional cultivation of *A. ferrooxidans* was conducted by using the same equipment but without the potential control, and presented as no bias-experiment.

The scheme of the experimental setup is shown in Fig. 1, which is made of a 250 mL storage bottle. The bias-experiment was carried out on a CHI1000a electrochemical workstation (Shanghai Chenhua Apparatus Corporation, China). Both the working and counter electrodes were graphite plate in the size of 7 cm×2.5 cm×0.5 cm and 7 cm×0.5 cm×0.5 cm, respectively, and the reference electrode was a saturated calomel electrode (SCE, 0.242 V vs. normal hydrogen electrode). By using modern-day technology, the potential of the working electrode was set to 0 V (vs. SCE). Since the redox potential of Fe^{3+}/Fe^{2+} is 770 mV (Rawlings, 2005) at pH 2.0, the reduction of Fe^{3+} at the working electrode was a spontaneous process. As a result, *A. ferrooxidans* could derive electrons and energy from the oxidation of Fe^{2+} to sustain its growth.

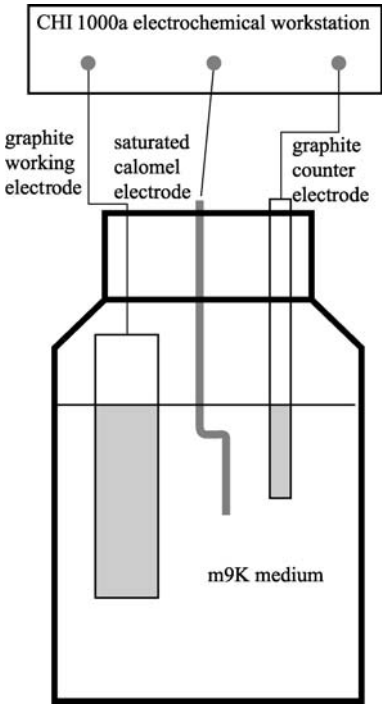

Fig. 1 Scheme of the experimental setup

2.3 Analytical methods and procedure

The acidity of the culture was measured using FE-50 pH meter (Mettler-Toledo, Swiss). The bacteria concentration was estimated by direct counting using a Helber Bacteria Z30000 cell counter (Thoma, UK) with 0.02 mm in depth and 1 mm^2 in area under a systematic microscope (Olympus BX41, Japan). The ferrous concentration was determined spectrophotometrically with *o*-phenanthroline method (Piwoni, 1992). Firstly, 1.25 mL of the culture medium was extracted and diluted to 50 mL in a standard colorimetric tube with deionized water. Then, 0.5 mL of

the diluted solution was spiked into another 25 mL standard colorimetric tube containing 5% *o*-phenanthroline (m/V) and acetic acid-ammonium acetate buffer. The mixture was adjusted to 25 mL with deionized water before analysis.

The precipitates in the culture were collected and dried in room temperature (25°C). After being ground into powder, the precipitates were subjected to analyses of their X-ray diffraction patterns (XRD), Raman spectroscopy and Fourier transform infrared (FTIR) spectroscopy, and observed under the environmental scanning electron microscope (ESEM).

The XRD analysis was carried out in a 12kV Rigaku-RA high power spinning anode X-ray diffraction apparatus (Rigaku, Japan) in a Microstructure Analytical Lab (Beijing) by using CuKα radiation (λ = 1.5406 Å). The precipitates were firmly packed in a glass holder and scanned from 10° to 70° with a speed of 4°/min.

Renishaw inVia Raman microscope with a 1K series He-Cd LASER system was applied for Raman spectroscopy. The sample was pressed between two triangle glass holders and then put into the microscope for testing. The Raman spectroscopy patterns of both the experimental group and the control were obtained with ten 10 s-scans and a single 10 s-scan, respectively, using 50×objective and 25% laser power set.

FTIR analysis was performed using BRUKER TENSOR 27 Fourier transform infrared spectroscopy (BRUKER, Germany). A small amount of sample powders and potassium bromide (spectroscopically pure) were both previously dried in desiccators, fully mixed in agate mortar, compressed into a transparent plate in a stainless holder and inserted into the FTIR instrument.

FEI Quanta 200FEG environmental scanning electron microscope (ESEM) equipped with an EDAX DX-4 EDS system was used to observe the micro-appearance and semi-quantitatively analyze the chemical compositions of precipitated minerals. Before observation, the precipitates were ultrasonically dispersed in a diluted ethanol solution for 5 min and then dropped on a silicon plate, which was attached to an aluminum holder by using conducting tape.

3 Results and discussion

3.1 Crystal morphology and chemical compositions

The precipitates generated in the two experiments were different from each other, in both morphology and composition. The precipitate obtained in the bias-experiment was yellow but red brown in the no-bias-experiment. The ESEM (Fig. 2) showed the precipitates in the bias-experiment (Fig. 2(a)) were well crystallized with a uniform size and shape. These particles presented a typical rhombohedron crystal of jarosite (Grishin et al., 1988). The ESEM of the precipitates in the no-bias-experiment (Fig. 2(b)) showed the presence of two minerals with crystal forms significantly distinguished from each other. One was well crystallized in a pseudo-cubic morphology, and the other showed needle-like aggregates with an average thickness of 130 nm covering the well crystallized mineral surface. The elemental compositions of the precipitates as analyzed by EDAX (energy dispersive analysis of X-rays) are shown in Table 1, which might be useful in identifying the precipitates.

As shown in Table 1, the Fe/S ratio of the rhombohedral crystals was 1.35 and 1.62 in the bias- and no-bias-experiment, respectively, close to the stoichiometric ratio of jarosite (Welch et al., 2008). In the no-bias-experiment, the Fe/S ratio of the needle-like aggregates was 3.77, which falls into the normal range of schwertmannite between 3.43–8 (Bigham et al., 1996; Liao and Zhou, 2007). The K/S ratio of the rhombohedral crystal was 0.32 in the bias-experiment, close to the theoretical value for the formula $KFe_3(SO_4)_2(OH)_6$, but was 0.05 in the no-bias-experiment, much less than the theoretical value for K-jarosite, indicating a possible substitution of part of the K^+ by NH_4^+ or H_3O^+. Given the above data, we speculated

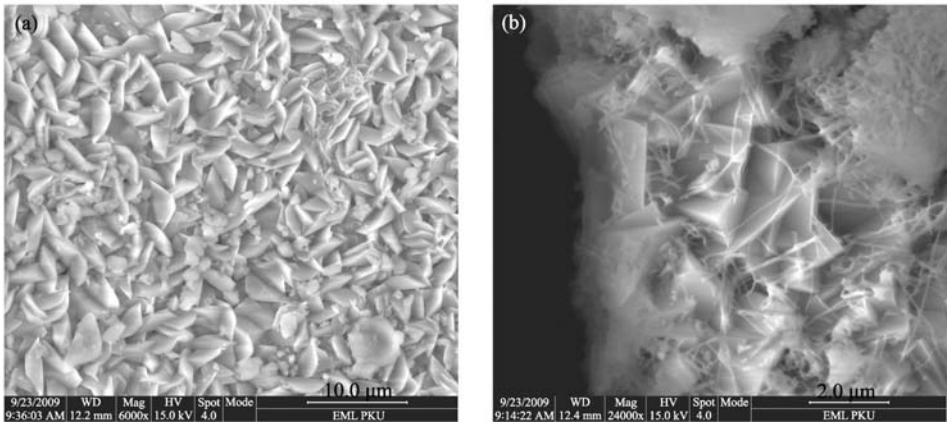

Fig. 2 ESEM images of the precipitates obtained in bias- (a) and no-bias-, (b) experiments

Table 1 Elemental analysis of the obtained precipitates

	bias-experiment	no-bias-experiment crystal	no-bias-experiment needle-like
Fe/%	13.53	16.18	19.93
S/%	10.01	10.01	5.28
O/%	72.16	72.97	74.79
K/%	4.30	0.85	(undetected)
Fe/S	1.35	1.62	3.77
K/Fe	0.32	0.05	/

that the crystal in the bias-experiment might be K-jarosite, while the well crystallized mineral formed in the no-bias-experiment was probably a solid solution of K-NH_4-H_3O jarosite. In addition, the needle-like aggregates in red brown were probably schwertmannite.

3.2 Crystal structure

The X-ray diffraction patterns (XRD) of the precipitates generated in the bias- and no-bias- experiments are shown in Fig. 3. Both of them showed the presence of the three strongest characteristic peaks at 2θ of 17.24°, 28.48° and 28.8°, corresponding to (012), (021) and (113) planes of K-jarosite (PCPDF No. 71-1777), respectively. This indicated that the precipitates generated in both experiments should be the jarosite-group minerals (referring PCPDF No. 71-1777, No. 26-1014 and No. 36-0425). By using UnitCell software, the crystal-cell parameters were calculated and are listed in Table 2. For the precipitates in the bias-experiment, the cell parameters were $a = 7.36$ Å, $c = 17.31$ Å and the cell volume was 811.95 Å^3, which were slightly larger than those in the standard PCPDF 71-1777 ($a = 7.315$ Å, $c = 17.22$ Å, $V = 798.17$ Å^3). Although the peak positions of the precipitates in XRD were identical in both the bias- and no-bias-experiments, the peak intensities were obviously different; those in the bias-experiment were stronger than in the no-bias-experiment, indicating the greater degree of mineral crystallinity in the bias-experiment.

3.3 Raman spectroscopy

The Raman spectra of the precipitates formed in the bias- and no-bias-experiments are shown in Fig. 4. Based on the parameters reported by Sasaki et al. (1998), the four peaks at 225, 300, 352 and 433 cm^{-1} were all assigned to the Fe-O bond. The peak at 570 cm^{-1} was attributed to γ(OH), and the predominant peaks at 1007, 456 and 626 cm^{-1} were probably a feature of SO_4^{2-}, which could be assigned to

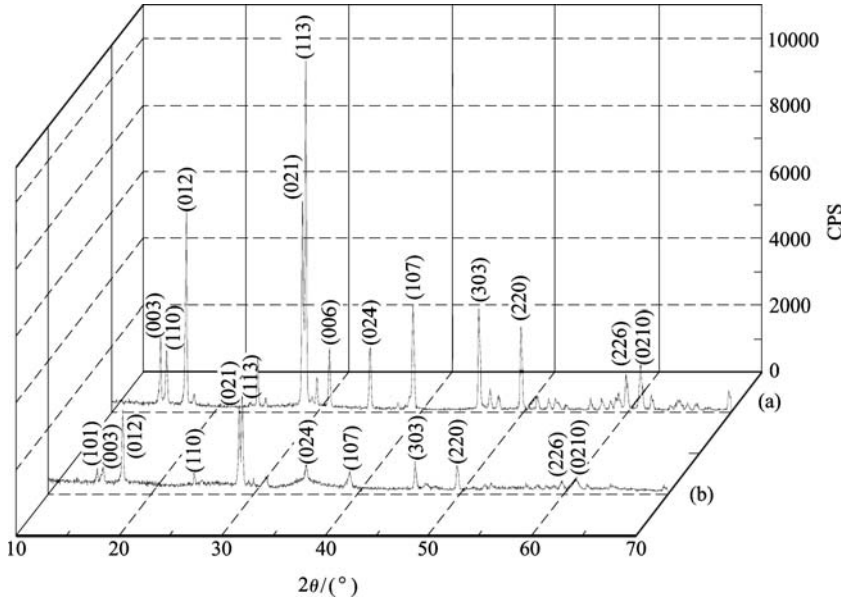

Fig. 3 XRD patterns of the precipitates generated in the bias- (a) and no-bias-, (b) experiments

Table 2 X-ray diffraction analysis of the precipitates obtained in the bias-experiment

		d value/Å		parameters/Å		V/Å^3
bias	5.1362 (012)*	3.1284 (021)	3.0953 (113)	$a = 7.36$	$c = 17.31$	811.64
no-bias	5.1370 (012)	3.1275 (021)	3.0953 (113)	$a = 7.36$	$c = 17.30$	811.95
PCPDF:22-0827	5.0900 (012)	3.1100 (021)	3.0800 (113)	$a = 7.29$	$c = 17.16$	789.77

* crystal faces are in parentheses

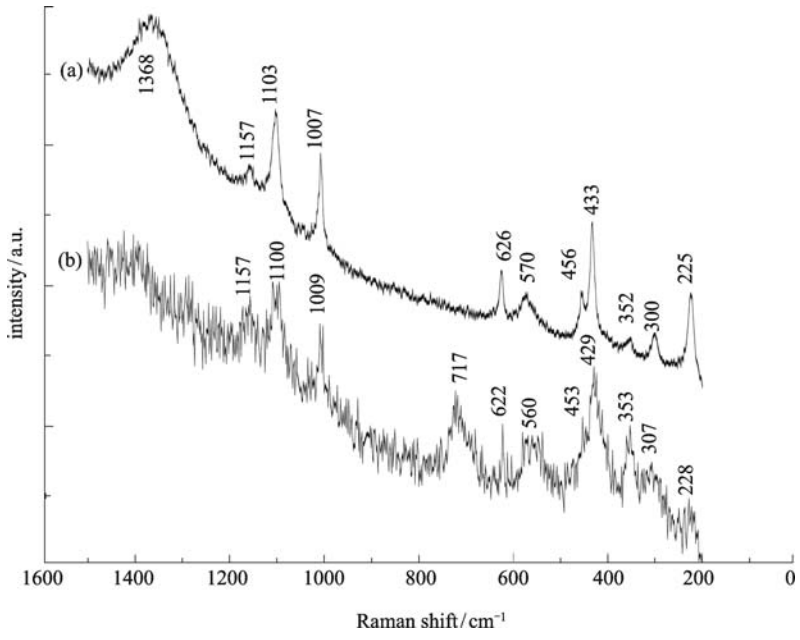

Fig. 4 Raman spectroscopy of the precipitates generated in the bias- (a) and no-bias-, (b) experiments

$\nu_1(SO_4^{2-})$, $\nu_2(SO_4^{2-})$ and $\nu_4(SO_4^{2-})$, respectively. The peaks at 1103 and 1157 cm^{-1} were both assigned to $\nu_3(SO_4^{2-})$. It should be noticed that the peak at 717 cm^{-1} in the no-bias-experiment assigned to ν_4 (SO_4^{2-}) in schwertmannite (Mazzetti and Thistlethwaite, 2002; Burton et al., 2009), was not observed in the bias-experiment. The results confirmed that schwertmannite was generated in the no-bias-experiment while it was not included in the bias-experiment.

3.4 FTIR Spectroscopy

Figure 5 showed the FTIR spectra of the precipitates formed in the bias- and no-bias- experiments. Both had a set of similar peaks. The strong absorption peak at around 3380 cm^{-1} was assigned to the O-H stretching, and the four absorption peaks in the wavenumbers of 628, 1004, 1086 and 1189 cm^{-1} were ascribed to ν_4, ν_1, ν_2 and ν_3 vibration of SO_4^{2-}, respectively. The two peaks at around 509 and 473 cm^{-1} were attributed to the vibration of FeO_6 coordination octahedron in jarosite (Liu et al., 2009). As compared with the bias-experiment, there was a unique peak at 1424 cm^{-1} in the no-bias-experiment (Fig. 5(b)), which was assigned to the ν_4 bending vibration of NH_4^+ (Sasaki et al., 1998). The appearance of this peak indicated the existence of NH_4-jarosite in the precipitates present in the no-bias-experiment. Notably, peak widening at 3380 cm^{-1} was observed in the precipitates harvested in the no-bias-experiment, which was probably caused by the presence of hydronium in the K site of jarosite (Basciano

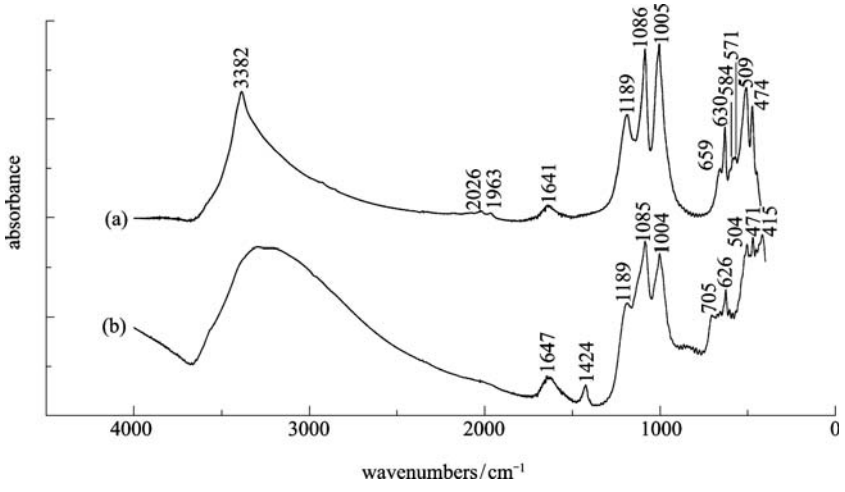

Fig. 5 FTIR spectra of the precipitates formed in the bias- (a) and no-bias-, (b) experiments

and Peterson, 2007). Further, the precipitates generated in the no-bias-experiment had two unique small peaks at 705 and 415 cm^{-1}, which were considered to be significant absorption bands representing the ν-FeO stretching vibration in schwertmannite (Regenspurg et al., 2003), which were reported to be only found in schwertmannite (Schwertmann et al., 1995). The FTTR spectra indicative of the identification of the precipitates are consistent with XRD, ESEM and Raman spectra.

3.5 Discussion

The ferrous, total ferric and *A. ferrooxidans* concentrations measured at a fixed interval of 24 hours in the bias- and no-bias-experiments are shown in Fig. 6.

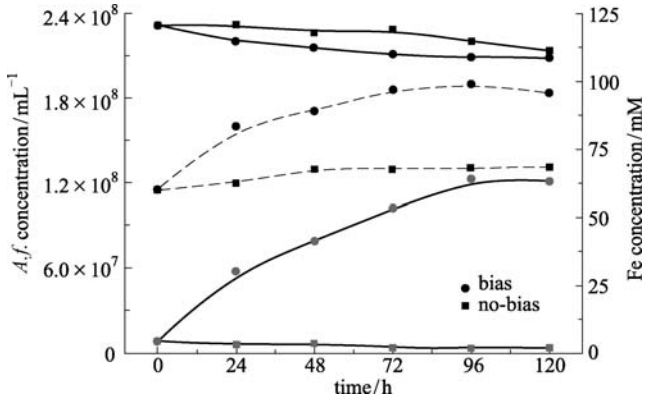

Fig. 6 *A. ferrooxidans* growth curves and ferrous/total ferric concentrations in the bias and no-bias experiments (black solid dots- ferric, gray solid dots- ferrous, solid lines- Fe concentration, dash lines- *A.f.* concentration)

The total ferric concentration was generally kept stable, with very little wastage in 120 hours due to the precipitation of ferric iron oxyhydrosulfate compounds. The ferrous concentration increased steadily from 4.44 to 63.2 mM in the bias-experiment while an obvious change in ferrous concentration could hardly be seen in the no-bias-experiment. Apparently, the continuous reduction of ferric ion to ferrous ion by external electrons resulted in a greater ferrous concentration in the bias-experiment. Further, it is generally accepted that a greater ferrous concentration sustains a more rapid growth of *A. ferrooxidans* (Matsumoto et al., 1999). A concomitant growth of *A. ferrooxidans* from 1.15×10^8 to 1.90×10^8 cells/mL in the bias-experiment was observed, which was due to a sufficient energy supply by external electrons, while a slight increase of *A. ferrooxidans* concentration was observed from 1.15×10^8 to 1.30×10^8 cells/mL in the no-bias-experiment.

All the minerals precipitated in the bias- and no-bias-experiment were influenced by the bioactivity of *A. ferrooxidans* in the m9K medium involving K^+, NH_4^+, H_3O^+, SO_4^{2-} and Fe^{3+}. The only difference between the two experiments was that a continuous electron flow was provided in the bias-experiment to successively reduce Fe^{3+} to Fe^{2+} in the culture solution. Thus, the precipitates formed in the bias- and no-bias-experiment had a distinct micro-appearance in ESEM (Fig. 2). In the bias experiment, the precipitate obtained was pure and uniform, which just included one single phase of the mineral. The mineral with a perfect crystal surface belonged to the trigonal system. By contrast, the precipitates formed in the no-bias-experiment included two kinds of minerals; one had a regular pseudo-cubic shape and the other was the needle-like aggregate.

The analyses of XRD, Raman spectra and FTIR indicate that the well-crystallized minerals in the bias- and no-bias experiments should be jarosite-group compounds. Although the degrees of crystallization were different, the XRD patterns of the two samples clearly indicated that both of them belonged to the jarosite-group compounds. The Raman and FTIR spectra showing the characteristic peaks of jarosite with tiny shifts (Sasaki et al., 1998) further supports the speculation. The presence of only three kinds of M^+ (M represents metal) in the culture solution (K^+, NH_4^+ and H_3O^+) suggests the formation of only three kinds of jarosite, i.e. K-jarosite, NH_4-jarosite and H_3O-jarosite. The identification of K by EDAX indicated the existence of K-jarosite in both experiments. By FTIR spectra, the N-H stretching vibration peak appearing at 1424 cm^{-1} was only detected in the no-bias-experiment sample, implying the existence of NH_4-jarosite, and the widening peak at 3380 cm^{-1} indicated the presence of H_3O-jarosite. Further, the Raman spectra of the no-bias-experiment precipitate had one distinct peak at 717 cm^{-1}, which was assigned to schwertmannite $\nu_4(SO_4^{2-})$ vibration mode (Mazzetti and Thistlethwaite, 2002; Burton et al., 2009). The FTIR spectra of the no-bias-experiment precipitates also showed the presence of two unique peaks at 705 and 415 cm^{-1}, corresponding to the ν-FeO stretching vibration and an unknown stretching vibration in schwertmannite, respectively (Schwertmann et al., 1995). As given by the data of Raman and FTIR, schwertmannite was found in a trace amount only in the no-bias experiment, consistent with the micro-appearance observed by ESEM. The observation of the needle-like aggregates covering on the surface of the pseudo-cubic crystals in the no-bias-experiment indicated that schwertmannite was precipitated after the formation of jarosite.

On the basis of the aforementioned points, the well crystallized minerals in the bias-experiment must be K-jarosite and possibly including H_3O-jarosite, while the well crystallized minerals in the no-bias-experiment must be a solid solution of K- NH_4-H_3O jarosite, and the poor crystallized needle-like aggregate should be schwertmannite.

It is interesting to note that a small difference in experimental conditions will lead to a dramatic change in precipitates. Bigham (1994) pointed out that schwertmannite formation was favored at the pH values of 3 to 4.5, and ferrihydrite or jarosite precipitation would be promoted with the higher or lower pH values. It was reported that schwertmannite also precipitated at the pH values ranging from 2.0 to 2.5 (Wang et al., 2006). In our experiments, both schwertmannite and jarosite could precipitate at the pH value of 2.0. Therefore, the pH value of the solution was not considered as a key parameter to control the precipitation of ferric sulfate. For the study of the mechanism, the variation of ion concentration in the culture medium during the experimental processes should be further investigated. The initial concentration of sulphate in m9K was sufficient (150 mM), while that of K^+ and NH_4^+ was as low as 1.04 mM and 1.8 mM, respectively. The ferric concentration was viable due to the experimental controls and bioactivity. In the bias-experiment, NH_4^+ acted as the only nitrogen source and was highly consumed by the rapid reproduction of *A. ferrooxidans*. Besides, a simultaneous reduction of Fe^{3+} to Fe^{2+} driven by the extra bias caused the concentration of Fe^{3+} to be relatively lower. Compared with the no-bias-experiment, the concentration of NH_4^+ and Fe^{3+} involved in the m9K solution in the bias-experiment seemed to be insufficient. Thermodynamically, the precipitation of Fe^{3+} as schwertmannite required the Gibbs free energy of -518.0 ± 2.0 kJ/mol (Majzlan et al., 2004), much higher than that of K-jarosite (-3313.7 kJ/mol) (Gaboreau and Vieillard, 2004). Thus, the low concentration of Fe^{3+} in the bias-experiment determined the preferential precipitation of K-jarosite over schwertmannite. In the no-bias-experiment, the concentration of *A. ferrooxidans* was almost kept at the original level. As a result, NH_4^+ was not depleted so fast as in the bias-experiment, and still remained constant in the solution. As no external electrons were input, the iron in the solution was in the state of Fe^{3+} and its concentration was almost 150 mM. Under the great concentration of Fe^{3+} and the relatively higher concentration of M^+, jarosite was easy to form. Since the Gibbs free energy of K-jarosite was more negative than that of NH_4^+-jarosite (Gaboreau and Vieillard, 2004), NH_4^+-jarosite could be formed only after K-jarosite. Referring to the difference in thermodynamics data between schwertmannite and jarosite, schwertmannite was thermodynamically unfavorable to precipitate compared with jarosite. Why did schwertmannite appear in the precipitates in the no-bias experiment? There was a hypothesis that sufficient ferric ions and M^+ ions were depleted out and no M^+ could participate in the formation of jarosite, resulting in the formation of schwertmannite. This hypothesis needs further confirmation and the follow-up experiments are in progress.

4 Conclusion

The precipitates generated during the *A. ferrooxidans* growth in the bias- and no-bias- experiments revealed distinctive differences due to the different growth statuses of *A. ferrooxidans* and Fe^{3+} in culture solutions. The culture solution of the bias-experiment had a low concentration of Fe^{3+} but a great concentration of *A. ferrooxidans*, which depleted NH_4^+ and thus only yielded the precipitate of K-jarosite. In the no-bias-experiment, the relatively low concentration of *A. ferrooxidans* existed in the culture solution, which resulted in a slight depletion of NH_4^+ and the great concentration of NH_4^+ and Fe^{3+}, leading to the precipitation of K-NH_4-H_3O jarosite and schwertmannite.

Acknowledgements This work was supported by the National Basic Research Program of China (No. 2007 CB815602).

References

Basciano L C, Peterson R C (2007). The crystal structure of ammoniojarosite, $(NH_4)Fe_3(SO_4)_2(OH)_6$ and the crystal chemistry of the ammoniojarosite-hydronium jarosite solid-solution series. Mineralogical Magazine, 71 (4): 427–441

Bigham J M (1994). Schwertmannite, a new iron oxyhydroxysulphate from Pyhäsalmi, Finland, and other localities. Mineralogical Magazine, 58: 641–648

Bigham J M, Schwertmann U, Traina S J, Winland R L, Wolf M (1996). Schwertmannite and the chemical modeling of iron in acid sulfate waters. Geochimica et Cosmochimica Acta, 60 (12): 2111–2121

Blake R C, Howard G T, McGinness S (1994). Enhanced yields of iron-oxidizing bacteria by in situ electrochemical reduction of soluble iron in the growth medium. Applied Environmental Microbiology, 60: 2704–2710

Burton E D, Bush R T, Johnston S G, Watling K M, Hocking R K, Sullivan L A, Parker G K (2009). Sorption of Arsenic (V) and Arsenic (III) to Schwertmannite. Environmental Science & Technology, 43 (24): 9202–9207

Colmer A R, Hinkle M E (1947). The Role of Microorganisms in Acid Mine Drainage: A Preliminary Report. Science, 106 (2751): 253–256

Colmer A R, Temple K L, Hinkle M E (1949). An iron-oxidizing bacterium from the acid drainage of some bituminous coal mines. The American Society for Microbiology, 59: 317–328

Drouet C, Navrotsky A (2003). Synthesis, characterization and thermochemistry of K-Na-H_3O jarosites. Geochimica et Cosmochimica Acta, 67 (11): 2063–2076

Dutrizac J E, Kaiman S (1976). Synthesis and properties of jarosite-type compounds. The Canadian Mineralogist, 14: 151–158

Gaboreau S, Vieillard P (2004). Prediction of Gibbs free energies of formation of minerals of the alunite supergroup. Geochimica et Cosmochimica Acta, 68 (16): 3307–3316

Grishin S I, Bigham J MTouvinen O H (1988). Characterization of

Jarosite Formed upon Bacterial Oxidation of Ferrous Sulfate in a Packed-Bed Reactort. Applied and Environmental Microbiology, 54 (12): 3101–3106

Liao Y H, Zhou L X (2007). Schwertmannite formed under extreme acid conditions and its environmental significance. Acta Petrologica et Mineralogica, 26 (2): 177–183 (in Chinese with English abstract)

Liu J, Tao X, Cai P (2009). Study of formation of jarosite mediated by thiobacillus ferrooxidans in 9K medium. Procedia Earth and Planetary Science, 1: 706–712

Majzlan J, Navrotsky A, Schwertmann U (2004). Thermodynamics of iron oxides: Part III. Enthalpies of formation and stability offerrihydrite ($Fe(OH)_3$), schwertmannite ($FeO(OH)_{3/4}(SO_4)_{1/8}$), and ε-$Fe_2O_3$. Geochimica et Cosmochimica Acta, 68 (5): 1049–1059

Matsumoso N, Nakasono S, Ohmura N, Saiki H (1999). Extension of Logarithmic Growth of Thiobacillus ferrooxidans by Potential Controlled Electrochemical Reduction of Fe(III). Biotechnology and Bioengineering, 64 (6): 716–721

Mazzetti L, Thistlethwaite P J (2002). Raman spectra and thermal transformations of ferrihydrite and schwertmannite. Journal of Raman Spectroscopy, 33: 104–111

Nakasono S, Matsumono N, Saiki H (1997). Electrochemical cultivation of thiobacillus ferrooxidans by potential control. Bioelectrochemistry and Bioenergetics, 43: 61–66

Piwoni M D (1992). Phenanthroline method. In: Greenberg AE, Clesceri LS, Eaton AD, eds. Standard methods for the examination of water and wastewater. Washington D C: American Public Health Association, p 3 (66)–63 (68)

Rawlings D E (2005). Characteristics and adaptability of iron- and sulfur-oxidizing microorganisms used for the recovery of metals from minerals and their concentrates. Microbial Cell Factories, 4: 13

Regenspurg S, Brand A, Peiffer S (2003). Formation and stability of schwertmannite in acidic mining lakes. Geochimica et Cosmochimica Acta, 68 (6): 1185–1197

Sasaki K, Tanaike O, Konno H (1998). Distinction of jarosite-group compounds by Raman spectroscopy. The Canadian Mineralogist, 36: 1225–1235

Schwertmann U, Bigham J M, Murad E (1995). The first occurrence of schwertmannite in a natural stream environment. European Journal of Mineralogy, 7: 547–552

Touvinen O H, Kelly D P (1973). Studies on the growth of *Thiobacillus ferrooxidans*: I. Use of membrane filters and ferrous iron agar to determine viable number and comparison with CO_2 fixation and iron oxidation measures of growth. Archives on Microbiology, 68: 285

Wang H M, Bigham J M, Jones F S, Tuovinen O H (2007). Synthesis and properties of ammoniojarosites prepared with iron-oxidizing acidophilic microorganisms at 22°C–65°C. Geochimica et Cosmochimica Acta, 71: 155–164

Wang H M, Bigham J M, Tuovinen O H (2006). Formation of schwertmannite and its transformation to jarosite in the presence of acidophilic iron-oxidizing microorganisms. Materials Science and Engineering C, 26: 588–592

Welch S A, Kirste D, Christy A G, Beavis F R, Beavis S G (2008). Jarosite dissolution II—Reaction kinetics, stoichiometry and acid flux. Chemical Geology, 254: 73–86